Journal of Materials Chemistry B

Extremophilic behavior of catalytic amyloids sustained by backbone structuring

Journal:	*Journal of Materials Chemistry B*
Manuscript ID	TB-ART-07-2022-001605.R1
Article Type:	Paper
Date Submitted by the Author:	15-Oct-2022
Complete List of Authors:	Beasley, Maryssa; Naval Research Laboratory Chemistry Division, Chemistry Dunkelberger, Adam; Naval Research Laboratory Chemistry Division, Chemistry Thum, Matthew; Naval Research Laboratory Chemistry Division, Chemistry Ryland, Elizabeth; Formerly at Naval Research Laboratory Chemistry Division, Chemistry Fears, Kenan; Naval Research Laboratory, Chemistry Grafton, Andrea; Formerly at Naval Research Laboratory Chemistry Division, Chemistry Owrutsky, Jeffrey; Naval Research Laboratory, Chemistry Division Lundin, Jeffrey; US Naval Research Laboratory, Department of Chemistry So, Christopher; Naval Research Laboratory Chemistry Division, Chemistry

Extremophilic behavior of catalytic amyloids sustained by backbone structuring

Maryssa A. Beasley,[1] Adam D. Dunkelberger,[2] Matthew D. Thum,[3] Elizabeth S. Ryland,[4,†] Kenan P. Fears,[5] Andrea B. Grafton,[4,†] Jeffrey C. Owrutsky,[2] Jeffrey G. Lundin,[6] and Christopher R. So[5,]*

AUTHOR ADDRESS

[1]NRC Postdoctoral Associate sited in Chemistry Division, Code 6176, U.S. Naval Research Laboratory, Washington, DC 20375-5342 USA

[2]Chemistry Division, Code 6121, US Naval Research Laboratory, 4555 Overlook Ave, SW, Washington, DC 20375-5342 USA

[3]NRC Postdoctoral Associate sited in Chemistry Division, Code 6124, U.S. Naval Research Laboratory, Washington, DC 20375-5342 USA

[4]NRC Postdoctoral Associate sited in Chemistry Division, Code 6121, U.S. Naval Research Laboratory, Washington, DC 20375-5342 USA

[5]Chemistry Division, Code 6176, US Naval Research Laboratory, 4555 Overlook Ave, SW, Washington, DC 20375-5342 USA

[6]Chemistry Division, Code 6124, US Naval Research Laboratory, 4555 Overlook Ave, SW, Washington, DC 20375-5342 USA

ABSTRACT

Enzyme function relies on the placement of chemistry defined by solvent and self-associative hydrogen bonding displayed by the protein backbone. Amyloids, long-range multi-peptide and -protein materials, can mimic enzyme functions while having a high proportion of stable self-associative backbone hydrogen bonds. Though catalytic amyloid structures have exhibited a degree of temperature and solvent stability, defining their full extremophilic properties and the molecular basis for such extreme activity has yet to be realized. Here we demonstrate that, like thermophilic enzymes, catalytic amyloid activity persists across high temperatures with an optimum activity at 81 °C where they are 30-fold more active than at room temperature. Unlike thermophilic enzymes, catalytic amyloids retain both activity and structure well above 100 °C as well as in the presence of co-solvents. Changes in backbone vibrational states are resolved *in situ* using non-linear 2D infrared spectroscopy (2DIR) to reveal that activity is sustained by reorganized backbone hydrogen bonds in extreme environments, evidenced by an emergent vibrational mode centered at 1612 cm^{-1}. Restructuring also occurs in organic solvents, and facilitates complete retention of hydrolysis activity in co-solvents of lesser polarity. We support these findings with molecular modeling, where the displacement of water by co-solvents leads to shorter, less competitive, bonding lifetimes that further stabilize self-associative backbone interactions. Our work defines amyloid properties that counter classical proteins, where extreme environments induce mechanisms of restructuring to support enzyme-like functions necessary for synthetic applications.

INTRODUCTION

Enzymes have long been sought to impart biological functions to synthetic materials in medical, food, textile, and sensing applications.[1, 2] Though some biological functions have been successfully incorporated into synthetic environments, proteins with intricate three-dimensional structures remain fragile outside of their natural environments. Weaknesses arise from the requirement that enzymes remain globular in their native aqueous biological environment to perform functions. Conversely, proteins which have achieved their ultimate aggregation state in solution maintain a fibrillar extended beta sheet structure known as amyloid. Nature relies on these materials to survive under extreme conditions: from tenacious bacterial biofilms, to the expansion of fungi, and even to the underwater attachment of barnacles.[3-5] In the synthetic realm, amyloids produced from proteins are often formed at high temperatures or in non-aqueous solvents,[6, 7] demonstrating that this class of materials would be ideal for performing functions in biologically extreme environments.[8] For catalytic amyloids, these functions can include catalyzing aldol reactions,[9] complex cascade reactions,[10] and oxidation of substrates like 2,6-dimethoxyphenol (DMP).[11] Recently, short septapeptides with rationally designed sequences exploit the amyloid backbone to assemble side-chains that coordinate catalytic metal centers to mimic the metalloenzyme carbonic anhydrase (CA).[12, 13]

Catalytic amyloids achieve turnover and catalytic efficiencies without extraneous globular protein elements. Amyloids maintain structure even with changes to their sequence, as demonstrated by Lengyel *et al.*, where copper containing analogs with a single residue substitution allowed for the reaction of phosphoester bonds.[14] Thus, these materials have also been explored

for their role as prototypical enzymes in early Earth environments,[8, 15] and shown to retain activity at elevated temperatures, pressures, and in non-aqueous solvents.[16-18] Most studies to date have examined catalytic activity at near ambient temperatures (below 40°C), and in mild co-solvent conditions.[12, 19] Applying high hydrostatic pressures (200 MPa) led to a 3.5 fold increase in reaction rate, while a slight temperature increase resulted in 130% rate enhancement.[19] Though promising, it is unclear what the optimum operating temperature of catalytic amyloids are, where such activity breaks down, or what mechanism the amyloid backbone undergoes in extreme environments to remain active.

Of the tools to interrogate protein structure, vibrational spectroscopy is commonly used to resolve secondary structures due to a direct response to amide bonds that define the backbone shape.[20] This allows infrared techniques to distinguish beta strands found in amyloid fibrils from those in free protein or in aggregated multi-protein oligomers.[21, 22] Previous studies have confirmed the extended beta sheet structure of catalytic amyloids up to 60 °C using linear FTIR transmission spectroscopy, though no major spectral transitions were observed.[19] More recently, two-dimensional infrared spectroscopy (2DIR) has yielded even greater structural information resulting from narrower linewidths and a non-linear sensitivity to highly organized structures typically convoluted by linear infrared techniques.[23-25] For example, the lowest amide I vibrational mode identified to date was discovered with 2DIR, and has been linked directly to unique amyloid structures of exceptional stability and organization.[25] 2DIR experiments are carried out in conventional FTIR liquid cells, which uniquely positions the technique to study varied amyloid structural states in extreme environments of high temperatures or non-aqueous solvents.

Here, we expand operational boundaries of catalytic amyloid materials to define where activity breaks down and apply advanced non-linear vibrational spectroscopy to probe how amyloid structures adapt in such environments. We choose a well-established model system consisting of the septapeptide [Ile-His-Ile-His-Ile-Gln-Ile] (Figure 1A), which is an ideal material for testing as the entire short sequence participates in the amyloid structure. We find that catalytic amyloid activity is greatly enhanced in heated aqueous environments up to at least 100 °C, with turnover rates ten-fold higher and a specificity constant almost 30-fold higher at its optimum over room temperature. 2DIR reveals an extraordinarily low frequency amide-I vibrational mode in heated water and in non-aqueous co-solvent environments absent in water at room temperature, which we ascribe to a structural reorganization to a more stable amyloid structure. Activity assays in 50% v/v co-solvent support this, with an ability to fully retain catalytic rates in solvents less polar than water, while those more polar are found to attenuate activity. Coupled with simulations of backbone hydrogen bonding lifetimes, we find that activity is facilitated by longer lasting hydrogen bonds created through a net loss of competition with water in non-biological environments.

MATERIALS AND METHODS

Materials

The peptide (Ac-IHIHIQI-amide, >99% purity) was synthesized by Vivitide (Gardner, MA). Percent purity is based on peak area calculated from HPLC analysis. $ZnCl_2$, Tris-HCl, and 4-nitrophenyl acetate (pNA) were purchased from Sigma-Aldrich (St. Louis, MO). Quartz cuvettes (GL14 cells) and silicon rubber septum used for the activity assays were obtained from Starna

Cells, Inc (Atascadero, CA). For atomic force microscopy (AFM) imaging, muscovite mica (Grades V5 and V1) was purchased from Ted Pella (Redding, CA).

Peptide preparation

Lyophilized peptide was prepared according to previously established protocols of amyloid-forming peptides.[26, 27] Briefly, peptides were dissolved in 100 μL hexafluoroisopropanol (HFIP) and sonicated for 10 min to break up preexisting aggregates. HFIP was evaporated off with a speedvac (Labconco, Kansas City, MO) to form dried peptide films. Peptide films were reconstituted in dimethyl sulfoxide (DMSO) for a final solution concentration of 10 mM peptide and sonicated for 10 min. DMSO stock solutions were stored at -80 °C to prevent aggregation. To induce fibrillization for experiments, 100 μM peptide was incubated in Tris buffer (50 mM Tris-HCl, pH=8.5) with 1 mM $ZnCl_2$. The peptide solution was incubated at room temperature for 2 h to form amyloid fibrils, with the time beginning immediately upon the addition of $ZnCl_2$. A 2 h wait period was selected to study the activity of the formed fibrils rather than the activity of the peptide during the process of fibril formation, as these activities have been shown to differ with catalytic amyloids.[28]

Characterization of peptide catalytic activity

Solutions of 4-nitrophenyl acetate (pNA) were prepared at 100 mM in acetonitrile and stored in a cool, dark environment. Immediately before each experiment, stored pNA solutions were diluted 100x in Tris buffer (pH=8.5, 1 mM $ZnCl_2$) to make fresh 1 mM pNA stock solutions. For activity assays, 20 μM peptide fibrils were incubated with the desired concentration of pNA in rubber septum-sealed quartz cuvettes with a pathlength of 2 mm. The absorbance of the hydrolyzed product (A_{400}) was recorded every 1 s for 10 min on a Lambda 1050 UV/Vis/NIR

spectrophotometer equipped with a PTP 1+1 Peltier temperature programmer. Controls consisting of pNA and buffer were run at each temperature and concentration to account for auto-hydrolysis of the substrate (Supplemental Figure S1), and the extinction coefficient of pNA at each temperature was measured (Supplemental Table 1). Initial velocity (V_0) was calculated for each substrate concentration and fit using nonlinear regression to the Michaelis Menten equation:

$$V_0 = \frac{V_{max}[S]}{K_m + [S]}$$

Michaelis Menten fits were used to determine the maximum velocity of the system (V_{max}), catalytic rate constant (K_{cat}), Michaelis constant (K_M), and the catalytic efficiency (K_{cat}/K_M) of the system.

Differential Scanning Calorimetry (DSC)

TA Instruments Discovery DSC (New Castle, DE) was employed to investigate amyloid phase transitions. Amyloids were formed by incubating 100 μM IHIHIQI peptide in Tris buffer with 1 mM $ZnCl_2$. Amyloids were pelleted via high-speed centrifugation and reconstituted in Tris buffer to form a 2% fibril solution. All samples were measured using high volume sample pans against a Tris buffer reference. The sample pans were loaded with 60 μL of an aqueous solution of the desired compound and the DSC equilibrated at 10 °C before a temperature ramp to 230 °C at a rate of 10 °C·min^{-1}. The sample was then cooled at a rate of 5 °C·min^{-1} to 10 °C and results were analyzed using TA Instruments TRIOS software. The minimum measurable transition was determined using free Lysozyme protein solutions. Lysozyme solutions were prepared and analyzed at 0.25 0.50, 1.0, 2.0 and 3.0 wt% respectively (Supplemental Figure S2). The denaturation of Lysozyme was observed as an endothermic transition at 82 °C. There was no

measurable transition below 1.0 wt % of lysozyme free protein suggesting that the system was unable to detect transitions of a similar energy at lower concentrations.

Temperature-dependent modeling

For all temperature model activity assays, 20 μM peptide fibrils were incubated at the desired temperature for 15 min, followed by immediate addition of 800 μM pNA. Here, $[S]>>>K_m$ so that the substrate was not a limiting factor in the reaction and the assumption can be made that $V_0=V_{max}$. Each experiment was performed in triplicate, and error bars indicate the standard deviation of the three trials. The absorbance of the product (A_{400}) was recorded every 1 s for 10 min on a Lambda 1050 UV/Vis/NIR spectrophotometer (Perkin Elmer) equipped with a PTP 1+1 Peltier temperature programmer, and the reaction rates were used to estimate the activation energy (E_A) of the system using the Arrhenius equation:

$$\ln(k) = \ln(A) - \frac{E_A}{RT}$$

where k is the rate constant, A is the pre-exponential factor, R is the gas constant, and T is the temperature.

The reaction rates were also plotted against temperature and fit to the macromolecular rate theory (MMRT) equation using non-linear regression. MMRT is defined as:

$$\ln(k) = \ln\left(\frac{k_B T}{H}\right) - \frac{\Delta H^{\ddagger}_{T0} + \Delta C_p^{\ddagger}(T - T_0)}{RT} + \frac{\Delta S^{\ddagger}_{T0} - \Delta C_p^{\ddagger}(lnT - lnT_0)}{R}$$

where k is the rate constant, k_B is Boltzmann's constant, h is Planck's constant, R is the gas constant, T is temperature, H is enthalpy, S is entropy, and C_p is the specific heat capacity.

Aggregate morphology characterization by atomic force microscopy

Ex situ atomic force microscopy (AFM) was used to image Ac-IHIHIQI-am aggregates formed under different conditions. The peptide was incubated for 2 h at room temperature to form fibrils, and the fibrils were then incubated at the desired temperature for 15 min. For imaging, 20 μL of the heated samples were deposited on freshly cleaved muscovite mica. Mica was preheated to the temperature of the fibril solution to prevent potential temperature-dependent changes in aggregate morphology upon deposition. After 2 min, the samples were rinsed with deionized water and dried under a gentle stream of nitrogen. Images were collected on a Keysight 9500 AFM system (Keysight, Inc., Tempe, AZ) at room temperature under acoustic isolation. All imaging was carried out in intermittent contact mode with scan rates between 1 and 2 Hz. High-resolution VTESPA-300 tips with a nominal spring constant of 42 N/m and a resonance frequency of 300 kHz were used. All image processing was performed with Gwyddion (Version 2.51, Czech Metrology Institute).

Attenuated Total Reflectance Fourier Transform Infrared Spectroscopy (ATR-FTIR)

Amyloid samples were formed by incubating 100 μM peptide in tris buffer (pH=8.5, 1 mM $ZnCl_2$) for 2 hours, and then 20 μL of fibril solution was deposited on a glass slide and dried with a gentle stream of air. In cases where the sample was heated, fibril solutions were held at the desired temperature for 30 minutes before deposition, and the glass slide was pre-heated to avoid cooling. Spectra were collected on a single-bounce diamond prism (Pike Technologies) using a Nicolet 6700 Spectrometer (ThermoFisher Scientific) equipped with an MCT-B detector that is cooled with liquid nitrogen. Background scans were collected with 256 scans, and controls consisted of tris buffer with 1 mM $ZnCl_2$ dried on a glass slide. 256 scans were collected for each

189 sample at 2 cm-1 resolution, and the prism was cleaned thoroughly with ethanol between each
190 sample.

191 **Two-dimensional infrared spectroscopy (2DIR)**

192 The 2DIR instrument has been described in detail previously.[29] Briefly, a commercial
193 Ti:sapphire laser (Coherent Astrella) provides 7 mJ, 35 fs pulses centered at 800 nm. We convert
194 a portion (3 mJ) of the 800 nm pulses to the mid-infrared *via* a commercial optical parametric
195 amplifier (Light Conversion) and subsequent difference frequency generation in $AgGaS_2$. A CaF_2
196 wedge reflects a small fraction of the mid-IR pulse to be used as the probe pulse and the transmitted
197 pulses are diverted to a commercial mid-IR pulse shaper (PhaseTech). The pulse shaper allows us
198 to generate pairs of mid-IR pump pulses with fine control over the relative delay (τ) and phase of
199 the two pulses. To optimize data collection and improve signal-to-noise, we employ phase cycling
200 to suppress scatter and use the pulse shaper to shift the signal with the rotating frame
201 approximation. The probe pulse traverses a computer-controlled delay stage that gives control over
202 its delay relative to the pump pulses (T_W). The pump and probe pulses intersect at the sample in a
203 pump-probe geometry after reflection from an off-axis parabolic mirror. After intersecting the
204 sample, the probe pulse is measured by a two-dimensional MCT array (PhaseTech) synchronized
205 with the 1 kHz repetition rate of the laser system, allowing us to measure the spectrum of each
206 laser shot. For a given value of T_W, we Fourier transform the τ-dependent nonlinear response at
207 each detection frequency to obtain the 2DIR spectrum.

208 The temperature of the cell windows (as measured by an infrared thermometer) lags the set
209 temperature reported by a thermocouple in the metal cell housing by 10-20 °C, depending on the
210 specific temperature. We report the 2DIR spectra in terms of the estimated sample temperature. At

temperatures above 100 °C, the sample remains liquid until the pressure overcomes the seals of the cell and large bubbles form as the water vapor escapes at around 180 °C. In the interest of rapid data collection as the temperature of the sample was elevated, we measured all spectra at a single waiting time, T_w = 0.2 ps.

Activity assays in organic solvents

Fibrils of IHIHIQI were incubated in 50% v/v solutions of ethanol, DMSO, or HFIP in buffer to determine if catalytic activity persisted in organic solvents. Amyloid fibrils were formed by incubating 100 μM peptide in Tris buffer with 1 mM $ZnCl_2$ for 2 hours. Amyloid fibrils were then diluted into a solution containing Tris buffer and the organic solvent of choice that contained $ZnCl_2$ to avoid diluting the final zinc concentration. The final conditions were 20 μM peptide, 50% Tris buffer, 50% solvent, and 1 mM $ZnCl_2$. To determine the impact of solution pH on activity, many conditions were systematically titrated with NaOH. For conditions including NaOH, 1 μL of the appropriate NaOH stock solution was added to each sample. Activity assays were initiated by introducing 200 μM pNA to the system and the absorbance (405 nm) was monitored every 55 seconds. Experiments were performed in Thermo Scientific clear bottom 96-well plates and data was collected using a Synergy H1 microplate reader. Controls consisting of pNA and Tris/solvent mixtures were run to account for different auto-hydrolysis rates of pNA in each solvent (Supplemental Figure S3). The initial velocity of each reaction was calculated at the linear portion of the kinetic curve.

Computational Analysis

Molecular dynamics (MD) simulations were performed on IHIHIQI assemblies in water, ethanol, DMSO, and HFIP with GROMACS (ver. 2021.1) using the CHARMM36 molecular

mechanics force field.[30] With the exception of HFIP, the solvents selected are fully parameterized in CHARMM36. Missing parameters for HFIP were calculated with Gaussian 16 using B3LYP[31] exchange–correlation functionalities and 6-311++G** basis set. Based on the model reported by Rufo et al.,[12] we constructed an initial model for the IHIHIQI assembly, which consisted of 12 parallel, extended β-strands in the upper and lower segments of the assembly (24 strands in total, Supplemental Figure S4). After solvation, molecular models underwent energy minimization using the steepest descent algorithm. Minimized systems were equilibrated by running a constant volume and temperature (NVT) ensemble for 1 ns, followed by a constant pressure and temperature (NPT) ensemble for 1 ns through a leap-frog time integration with 1 fs time steps, while heavy atoms in peptides were constrained. In all simulations, bond lengths between hydrogens and heavy atoms were constrained using the LINCS algorithm.[32] For production simulations, NPT ensembles were performed for 1-2 μs with all heavy atoms allowed to freely move. The average hydrogen bond lifetimes were extracted from the autocorrelation function according to the Luzar and Chandler method and summarized in Table 1.[33]

RESULTS

Catalytic amyloids have thermophilic properties with an optimum temperature between 80 and 85 °C. To determine the extent of thermophilic activity, we first assemble amyloids from the septapeptide IHIHIQI (Figure 1A) and then expose them to p-nitrophenyl acetate (p-NA) at temperatures ranging from 25 °C to 100 °C. Upon cleaving the ester bond to remove acetate, p-NA becomes the colorless product p-nitrophenol (p-NP) which turns yellow when deprotonated into p-nitrophenolate. Using a fixed peptide concentration, we utilize a Michaelis-Menten fit (Figure 1B) to determine the maximum velocity V_{max}, catalytic turnover k_{cat}, Michaelis constant

K_M, and the specificity constant k_{cat}/K_M for catalytic amyloids at four increasing temperatures. At 25 °C, we observe similar values as reported previously with a k_{cat} of 0.023 s^{-1} and K_M of 0.52 mM (Figure 1D, F).[12, 16, 18] Interestingly, the activity increases monotonically until approaching 75 °C where k_{cat} and V_{max} are enhanced by an order of magnitude (Figure 1C, 1F), but then falls as the temperature approaches 100 °C. While k_{cat} increases up to 75 °C, a decreasing K_M over the same temperature range yields a sharp 30-fold increase in specificity constant to 1305 $s^{-1}\cdot M^{-1}$ at 75 °C from 44 $s^{-1}\cdot M^{-1}$ at room temperature (Figure 1G). Despite a loss of activity at very high temperatures, the specificity constant continues to increase up to 100 °C. Curved activity (k_{cat}) over operating temperatures is typical in natural enzyme systems,[34] where the maximum is defined as the optimum temperature T_{opt} and this value identifies the operating range as phsycrophilic (low temperature), mesophilic (medium temperature), or thermophilic (high temperature). Loss of activity above T_{opt} has historically been related to the melting transition (T_m) of the protein, when T_m overlaps with T_{opt}. However, many enzymes exhibit melting points well above their T_{opt} temperature.[34, 35] Typical enzymes operate optimally between 37 and 50 °C, and the T_{opt} between 80 and 85 °C for peptide assemblies defines catalytic amyloids as thermophilic.

Catalytic amyloids exhibit curved temperature response fit by thermodynamic modeling. We next determine the nature of the optimum temperature curve we observe with catalytic amyloids. To explore this behavior, we measure activity from 25 to 100 °C at 5 °C increments and again find that the activity follows a distinct curve with maximum activity between 80 and 85 °C (Figure 2A). Attempting to derive activation energy, E_a, by fitting the activity curve with the Arrhenius equation expectedly yielded poor results due to the curvature of $\ln(k_{cat})$ plotted against 1/T (Figure

2A). Applying linear regression to the k_{cat} values from a low, narrow temperature range (25 °C – 40 °C) as previously done by others[19] yields a similar E_a of 57 ± 4 kJ/mol (compared to 60 ± 3 kJ/mol) with an R^2 value of 0.95 (Figure 2A). However, extending the temperature range to include k_{cat} values up to the point of maximum activity (25 °C – 80 °C) results in a ~23% decrease of E_a to 44 ± 2 kJ/mol. When the entire temperature range is considered (25 °C – 100 °C), the E_a decreases even further to 32 ± 1 kJ/mol. Under the Arrhenius framework, E_a should not change when varying the temperature until the point where protein denaturation occurs. To determine if the activity curve is from fibril denaturation, differential scanning calorimetry (DSC) was performed in the temperature range of the activity assay and yielded no major transitions (Figure 2B). In addition, AFM images of the sample heated to 100 °C demonstrate that the amyloid materials are still present and are similar in morphology to those at 25 °C (Figure 2C). IHIHIQI fibrils at room temperature are short in height and relatively wide, presenting as a belt-like fibril morphology. These belt-like aggregates can bundle together to form larger fibril structures (Figure 2C) as previously shown. Fibrils heated to 100 °C maintain that same morphology, with larger fibril bundles consisting of primarily smaller belt-like fibrils. Thus, a drop in activity cannot be correlated with denaturation or any major instabilities when materials are exposed to elevated temperatures.

Generally, it is thought that thermophilic enzyme behavior obeys an exponential Arrhenius relationship with temperature until the protein denatures, at which point such a relation breaks down. In systems where denaturation is not occurring, other thermodynamic models must be considered. Recently, a framework has been developed that expands upon the Arrhenius equation and demonstrates that enzymes can experience decreases in activity at high temperatures independent of denaturation.[36, 37] Macromolecular Rate Theory (MMRT) considers the

thermodynamic parameter specific heat capacity (ΔC_p), which relates to macromolecular dynamics and quantifies the temperature dependence of the enthalpy and entropy of a system. When considering k_{cat} values across the entire temperature range of the activity assay, MMRT gave superior fits to the data compared to the Arrhenius equation (R^2=0.93 vs R^2=0.75, respectively) (Figure 2D). Where Arrhenius predicts a constant acceleration in k_{cat} at temperatures below enzyme denaturation, our materials experience a decline in rate acceleration true to the MMRT model. This results in a temperature, defined as T_{opt}, where the catalytic activity is at its maximum potential value. Fitting our data to the MMRT equation reveals T_{opt} for these materials to be 81.3 ± 3 °C, which classifies these materials as thermophilic with temperature sensitivity parameters similar to naturally occurring thermophilic enzymes. One of these parameters, ΔC_p, can be derived by fitting the data to MMRT and typically spans values ranging from -11 to 0 kJ/mol. Materials with a ΔC_p closer to 0 have a broad activity curve that covers a wide range of temperatures, while materials with lower ΔC_p values have sharper, narrower activity curves. The ΔC_p for these materials is -2.02 ± 0.01 kJ/mol K, indicating that the materials maintain a high level of activity over a wide temperature range including lower, physiologically relevant temperatures even when maintaining a high T_{opt}.

2DIR spectroscopy reveals restructuring of backbone hydrogen bonds at elevated temperatures. To gain insight into the structural changes that occur at elevated temperatures and accompany the change in activity, we employ 2DIR in a temperature-controlled demountable liquid cell. We begin with the room-temperature spectrum of IHIHIQI in D_2O (Figure 3A), measured 0.2 ps after excitation (T_w = 0.2 ps). In 2DIR spectroscopy, the nonlinear response of the system is displayed as a function of the probe or measurement frequency (here, on the x-axis) and the pump or excitation frequency (y-axis). In the simplest case, a vibrational band appears as

a negative signal along the diagonal, where the pump and probe frequencies are equal, accompanied by a positive signal at lower probe frequency. This positive feature is the anharmonically shifted excited-state absorption of the band. The strongest feature in the spectrum at room temperature occurs at 1625 cm^{-1} and corresponds to the amide-I stretching band (primarily C=O stretch with some contribution from the C—N stretch and N—H bend) of the IHIHIQI fibrils (indicated with a solid black outline in Figure 3A). These spectra broadly match peaks observed when samples are dried and characterized by conventional ATR-FTIR (Figure 3, black curves), where the amide I region of similarly heat treated samples contain a dominant peak centered at 1628 cm^{-1}, within the 1620-1630 cm^{-1} region known to correspond to amyloid backbone structures. In general, lower frequency bands can often correspond to more highly ordered amyloid structures with stronger coupling between the oscillators that make up the collective amide-I band, but subtle changes in the relative arrangement of the C=O moieties can give rise to appreciable frequency shifts.

The main feature discussed above is considerably elongated along the diagonal region of the 2DIR spectrum, but we use the cross peaks present in the spectrum to determine the source of this elongation. Cross peaks appear when exciting one vibrational band induces a response in another *via* myriad pathways, including anharmonic coupling and energy exchange. That the cross peaks exist at T_w = 0.2 ps suggests that the oscillators are anharmonically coupled to one another. One class of the cross peaks we observe, outlined by solid black lines (ω_{pump} = 1625 cm^{-1}, ω_{probe} = 1635 cm^{-1} and designated 1625/1635 in Figure 3A-C), indicates coupling between the main amide-I mode and a much weaker broad absorption band at slightly higher frequencies. We speculate that this band indicates a small contribution to the spectrum from a less ordered region of the fibrils. The second, and by far more interesting, cross peak (indicated by a dashed black outline in Figure

3A-C) occurs at lower frequencies (1612/1625), consistent with a highly ordered amyloid structure. The presence of these cross peaks implies that the elongation of the main feature centered at 1625 cm^{-1} arises, at least partially, from the presence of the diagonal peaks that contribute to the cross peaks. From the frequencies of the cross peaks we determine that these smaller features occur at 1612 cm^{-1} and 1635 cm^{-1}. In total, the room-temperature spectrum indicates a well-ordered amyloid structure with some smaller fraction of both higher- and lower-frequency absorbing structures. We infer from the presence of cross peaks between the smaller features and main feature that these structures exist simultaneously in a given fibril and not, for instance, that there are several fibrils with varying degrees of order contributing to the spectrum.

We next examine how the 2DIR spectrum changes as the sample cell is heated from room temperature to 130 °C (Figure 3). We observe two distinct regimes of spectral evolution, with representative spectra shown (Figures 3B and 3C). When heated to 100 °C, samples characterized by ATR-FTIR are largely unchanged with the amide I peak still centered at 1628 cm^{-1} (Figure 3B). On the other hand, the main feature in the 2DIR spectra at 1625 cm^{-1} has narrowed and shifted slightly (*ca*. 2 cm^{-1}) to higher frequency upon heating to 100 °C, with a 10% decrease in signal intensity. This narrowing and shifting makes the low-frequency feature at 1612 cm^{-1}, whose presence we inferred from the presence of the 1612/1625 cross peak at RT, much more readily apparent along the diagonal. At 130 °C the 1625 cm^{-1} feature clearly begins to weaken but the 1612 cm^{-1} feature becomes more intense. Critically, we take the survival and intensification of the low-frequency mode as evidence that the amyloid structure is preserved even under these extreme temperature and pressure conditions. Even if the low-frequency mode does not report on a more ordered structure compared to the main feature, its survival indicates that a high degree of order is preserved at high temperatures. If, on the other hand, the entire nonlinear signal were disrupted

by cell expansion or the fibrils denatured, we would expect both features in the spectrum to disappear simultaneously or to show rapid conversion to a higher frequency 1665 cm^{-1} mode that corresponds to random-coil secondary structure.

To better visualize the evolution of the 2DIR spectrum as a function of temperature, we compute and plot the volumes of the main 1625 cm^{-1} feature integrated from 1620 cm^{-1} to 1630 cm^{-1} along the pump and probe axes and the smaller 1612 cm^{-1} feature integrated from 1610 cm^{-1} to 1615 cm^{-1} (Figure 3D). To highlight changes in the peak volumes we perform two distinct subtractions. First, we subtract the signal integrated from 1615 cm^{-1} to 1620 cm^{-1} from the 1612 cm^{-1} to remove contributions from the low-frequency edge of the main feature at low temperatures. Second, we subtract the room-temperature value of the integrated intensity from each subsequent value to find a differential peak volume that illustrates the change in intensity as a function of temperature. We report the unsubtracted integrated intensities in Supplemental Figure S5. The volume of the main feature decreases monotonically with temperature while the volume of the 1612 cm^{-1} feature remains constant and then increases after 100 °C. The ratio between the two features increases from about 0.07 at room temperature to 0.13 at 130 °C (Supplemental Figure S5B). We deduce from these results that at high temperatures the fibrils undergo a restructuring that slightly favors the conformation that gives rise to the 1612 cm^{-1} compared to room temperature. In this way, 2DIR spectroscopy serves to demonstrate that the amyloid structure survives and, if the lower frequency band indeed corresponds to more a more highly ordered substructure, becomes better ordered as the temperature increases. The loss in activity at high temperatures cannot, therefore, be attributed to a loss of backbone structure.

Catalytic amyloids undergo structuring in organic solvents. As catalytic amyloids have demonstrated activity in the presence of mild dilute solvents,[16, 17] we use 2DIR to resolve subtle changes in backbone hydrogen bonding for 100% solvent conditions. Of the solvents discussed above, ethanol, DMSO, and HFIP have spectral windows of transmission that allow us to measure 2DIR spectra. In all three solvents, the spectrum exhibits a two-peaked structure qualitatively similar to that we observed at high temperatures in D_2O (Figure 4A-C). Both the main amyloid amide-I feature and the low-frequency feature along the diagonal are shifted to higher frequency by a few cm^{-1}. We interpret this shift as the result of the solvatochromism of the amide-I mode, which has been extensively studied both experimentally and theoretically.[38, 39] The shifts we observe are significantly smaller than reported for n-methyl acetamide in ethanol and DMSO solution, but we expect that the amide moieties of the IHIHIQI backbone to sample less of the solvent electrostatic environment because of their placement in the strongly ordered amyloid structure.

In addition to 2D IR, AFM microscopy was utilized to examine fibril morphology in the three solvent systems. In DMSO, individual fibrils are similar in morphology to those observed in 100% tris buffer. However, the exposure to solvent does change the bundling of the fibrils; in DMSO, fewer fibril bundles are observed, and there is a significant increase in the number of individual, discrete sheet-like species (Figure 4D inset). In ethanol, fibrils formed large bundles as they did in tris buffer (Figure 4E). In both DMSO and ethanol, fibrils maintained a belt-like morphology similar to tris buffer when observed at higher magnification (Figure 4G), supporting the 2DIR data that materials are still organized as amyloids in cosolvent environments. Very few amyloid fibrils were observed in any image of IHIHIQI fibrils exposed to HFIP (Figure 4F).

Catalytic amyloids retain activity in 50/50 vol% co-solvent environments. With evidence of the amyloid backbone surviving in non-aqueous solvents, we then set out to determine how those solvents affect catalytic activity. Activity of IHIHIQI was measured in 50/50 vol% co-solvent mixtures of Tris with DMSO, ethanol, or HFIP and the initial velocity was compared to activity measured in 100% Tris buffer. In the co-solvent mixtures, activity of catalytic amyloids exhibited a large degree of variation depending on the solvent (Figure 5A-C). While lower than the activity level in tris buffer, the catalytic amyloids maintained high levels of activity in both DMSO and ethanol co-solvent mixtures. However, no product formation was observed in HFIP co-solvent mixtures. The decrease in product formation observed in the solvent mixtures could be due to factors other than loss of fibril structure. Metal coordination is pH-dependent due to two protonation/deprotonation steps of histidine side chains,[11, 12] and as a result the catalytic activity significantly decreases with pH (Supplemental Figure S6). In addition, to monitor product formation with a colorimetric assay, the product (p-nitrophenol) must be deprotonated to p-nitrophenolate. Therefore, both product formation and product detection can be hindered by low levels of OH^-. To see if altering the hydroxide concentration could restore activity in the non-aqueous solvents, activity was measured in 50/50 vol% Tris/solvent mixtures that were systematically titrated with NaOH (Figure 5A-C). Activity of the catalytic amyloids in 50/50 vol% tris/DMSO increased with additions of NaOH (Figure 5A), reaching 78% of the reaction rate in tris buffer upon addition of 1 mM NaOH (Figure 5D). Further addition of NaOH resulted in high background hydrolysis and thus were not considered reliable (Supplemental Figure 3). Titration of NaOH to tris/ethanol mixtures resulted in subtle changes to the kinetic curves (Figure 5B), but when corrected with the appropriate background rates of hydrolysis there was no observed increase in reaction rate (Figure 5D). In HFIP, there is little to no activity observed regardless of added

NaOH (Figure 5C). The restoration of catalytic activity by NaOH titration in the DMSO and ethanol co-solvent mixtures indicates that the amyloid backbone remains intact and structured, and the decrease in observed activity is likely due to interactions with the sidechains and histidine triad rather than the backbone. When the hydroxide concentration is controlled, activity can be restored to levels similar to rates in Tris buffer.

Backbone-to-backbone hydrogen bonding lifetimes increase in organic solvents. We performed molecular dynamics (MD) simulations to assess the stability of the quaternary structure of the peptide assemblies in the various solvent systems. Simulations began with the idealized structure of an IHIHIQI fibril, consisting of a bilayer of extended sheets with isoleucine residues displayed in the interior of the fibril. Molecular models of IHIHIQI fibril were solvated in the pure solvent systems, rather than 50/50 vol % aqueous-organic, to increase the likelihood of observing destabilization events during the microsecond timescale of simulations. Table 1 shows the average lifetime of hydrogen bonds forming between neighboring solvent molecules, solvent molecules and peptides, and the amide backbones of neighboring peptide strands. In all four solvent systems, the lifetimes of solvent-peptide bonds were 1 or 2 orders of magnitude greater than solvent-solvent bonds, and backbone-backbone bonds 1 or 2 orders of magnitude greater than solvent-peptide bonds. These results indicate backbone-backbone hydrogen bonding is more stable than solvent-peptide hydrogen bonding, as is supported by the experimental observations of fibril formation.

Table 1. Hydrogen bonding lifetimes (ns) in various solvent environments.

Solvent Environment	Backbone-to-Backbone (ns)	Solvent-to-Peptide (ns)	Solvent-to-Solvent (ns)
Water, 300K	7.1	0.014	0.002
Water, 400K	1.1	0.014	0.002
Ethanol, 300K	15.9	0.14	0.03

Dimethyl Sulfoxide, 300K	36.0	1.5	--
Hexafluoro-2-propanol, 300K	76.5	1.9	0.06

More importantly, the backbone-backbone hydrogen bonding lifetimes increase in the following order, H_2O < ethanol < DMSO < HFIP, suggesting the network of hydrogen bonds linking the beta-sheets along the fibril axis are more stable in organic solvents. We note the peptide bilayer quaternary structures also persisted in H_2O, DMSO, and ethanol, however; the hydrophobic core became solvated in HFIP and the upper and lower segments separated while retaining the secondary structure of the peptide strands (Supplementary Figure S4). Therefore, differences in the quaternary structure of IHI in Tris/HFIP could be a factor in its lower catalytic activity compared to the other solvent systems.

DISCUSSION

Catalytic amyloids assembled from short septapeptides demonstrate curved thermophilic temperature-dependent behavior typically found in natural enzymes and exhibit a T_{opt} of 81°C. This allows us to place enzyme mimics amongst their natural carbonic anhydrase (CA) counterparts. Bovine carbonic anhydrase (bCA II) maintains optimum activity at 60 °C, while variants isolated from thermophilic bacteria display optimum activity at up to 80 °C.[40, 41] Our measurement of T_{opt} at 81 °C places *de novo* designed peptides at the extreme of naturally discovered anhydrases, 33% higher than bCA II. Gain of activity as a function of temperature in catalytic amyloids is similar to those observed in thermophilic CA variants, where amyloids exhibit a ten-fold enhancement at T_{opt} over room temperature compared to 6-7 fold enhancements for bCA II.[40] Counter to natural enzymes, we observed minimal denaturation at the T_{opt} and higher temperatures which led to use of the MMRT model to describe decreasing activity. The high

correlation coefficient found by MMRT modeling supports our observation by calorimetry, 2DIR spectroscopy, and AFM that these materials exhibit no denaturation or loss of backbone structure at high temperatures or in non-aqueous co-solvents. There is also a strong agreement between structural properties of this material and the temperature sensitivity parameters derived with MMRT. The measured ΔC_p of this material from modeling is similar to that of naturally rigid thermophilic enzymes and correlates well with the low system flexibility of the amyloid structure. In addition, the relationship between temperature sensitivity parameters T_{opt} and ΔC_p correlates well with other thermophilic enzymes that follow the MMRT model.[36, 37] Loss of function through dissociation of zinc from histidine at elevated temperatures is not believed to be responsible for their activity breakdown, as analogous CA thermophiles exist with the same active site that operate at high temperatures. Further, excess zinc in our activity assays fill in for the increased dissociation constant of zinc to CA at higher temperatures.[42]

Narrow lineshapes resolved by 2DIR have brought new molecular insight into how catalytic amyloids adapt to extreme environments. The presence of additional lower frequency satellite modes in the 1610-1620 cm^{-1} amide I range and their preference for high temperatures and organic solvents further demonstrates that catalytic amyloids retain highly ordered structures in extreme environments. This mode coincides with that of a similar frequency found in the insoluble portion of aggregates generated from the Amyloid-beta protein, which was identified to be the lowest infrared frequency absorbed by the backbone.[25] Subtle transitions in the low amide range have only been observable by 2DIR, as previous linear FTIR analysis of catalytic amyloids found no change in vibrational spectra when heated to 60 °C.[19]

Contrary to typical protein behavior, 2DIR spectroscopy and AFM show that catalytic amyloids studied here do not denature upon exposure to high temperatures or non-aqueous solvents of lesser polarity. Our results indicate the opposite— that IHIHIQI amyloids subtly restructure to favor low-frequency absorption features that may indicate more highly ordered structures in extreme environments. Owing to their low area to volume ratio, peptide structure is defined mainly as the competition between backbone and solvent hydrogen bonding.[43] Propensity of folding is often defined by the percentage of non-polar solvent in water which induces self-associative structural transitions.[43-45] In the case of pre-formed amyloids, backbone hydrogen bonding may be enhanced due to the displacement of water by less competitive co-solvents or shorter bonding lifetimes experienced in solvents and at high temperatures. Simulations of short amyloid structures constructed of septapeptides demonstrated that hydrogen bonding lifetimes along the backbone were two-, five-, and ten-fold longer in ethanol, DMSO, and HFIP, respectively, than water at 300 K (27 °C). While hydrogen bonding between peptide strands is stable in aqueous and organic solvents, HFIP solvated the hydrophobic core of the peptide bilayers leading to their separation in MD simulations. These results support the finding that activity did not persist in HFIP (Figure 5E). At high temperatures (water at 400 K, 127 °C), hydrogen bonding lifetimes decreased seventeen-fold while activity is observed to enhance by ten-fold. While solvent activity relies on the protonation state, temperature dependent enhancements may instead be largely due to Arrhenius-type behavior. Our experiments and simulation highlight new mechanisms that amyloid materials undergo as extremophilic materials, in which backbone interactions become more stable in response to non-aqueous environments.

CONCLUSION

A new mechanism is observed for catalytic amyloid materials that facilitates enzyme-like activity when placed in extreme solvents and temperatures up to 100 °C. Restructuring to stable backbone hydrogen bonds in these environments leads to full catalytic activity in less polar co-solvents and enhancements by an order of magnitude at high temperatures. We categorize catalytic amyloids studied here as both thermophilic and extremophilic in behavior, remaining active in environments that conventional enzymes denature. These properties highlight amyloids as a robust platform for the design of new enzymatic functions for use in harsh non-biological environments.

FIGURE CAPTIONS

Figure 1. Molecular structure and temperature dependent activity of catalytic amyloids formed from IHIHIQI. (A) Structure of the IHIHIQI peptide (left), along with structures of the assembled catalytic amyloids (center, right). (A) Initial velocity v_0 as a function of p-nitrophenyl acetate concentration across temperatures (red, 25 °C, blue, 50 °C, orange, 75 °C, green 100 °C), (B) V_{max} calculated as a function of temperature, (C) Michaelis constant (K_M) as a function of temperature, (D) Arrhenius relation plotted as 1/T versus ln(k_{cat}), (E) Catalytic turnover (k_{cat}) calculated as V_{max}/[IHIHIQI] plotted across temperature, and (F) catalytic efficiency of catalytic amyloids showing optimum at 75 °C. Peptide concentration is 20 μM in all cases, and substrate concentrations include 12.5, 25, 50, 100, and 200 μM. All experiments performed in triplicate.

Figure 2. Catalytic amyloids maintain structure and function at high temperatures. (A) Temperature-dependent activity curves fit to the Arrhenius equation to derive the activation energy. Dashed lines represent linear fits for the activity curve in the temperature range 25-50°C (yellow), 25-80 °C (green), and 25-100 °C (blue). (B) DSC curve of IHIHIQI fibril solution. (C) Representative AFM images of fibrils at room temperature (top) and 100 °C (bottom), with zoomed images presented on the right. (D) Same activity data as (A) fit to the MMRT equation. Experiments were performed in triplicate and error bars for the activation energy represent the standard deviation.

Figure 3 Linear IR (top) and 2DIR (bottom) spectra of IHIHIQI in D_2O recorded at cell temperatures (A) 25 °C, (B) 100 °C and (C) 130 °C. The contour line spacing is unequal with more contours between values of -0.1 and 0.1 to accentuate small features in the spectra. The solid black boxes highlight the cross peak denoted 1625/1635 in the text and the dashed black boxes highlight the cross peak denoted 1612/1625. (D) Differential peak volume computed as described in the

main text of the two main features at 1625 cm^{-1} (blue) and 1612 cm^{-1} (red) as a function of the temperature of the cell.

Figure 4. Structure of catalytic amyloids in non-aqueous co-solvents. 2DIR spectra of IHIHIQI in (A) DMSO, (B) ethanol, and (C) HFIP. The contour line spacing is unequal with more contours between values of -0.1 and 0.1 to accentuate small features in the spectra. Representative AFM images of IHIHIQI in (D) DMSO, (E) ethanol, and (F) HFIP. The box-in portion in panel (D) has a smaller height scale in order to see the shorter aggregates more clearly. (G) Belt-like amyloid fibrils of IHIHIQI present in 50/50 vol% tris/DMSO, tris/EtOH, and 100% tris buffer.

Figure 5. Activity of catalytic amyloids in non-aqueous co-solvents. Activity of IHIHIQI fibrils toward pNA in 50/50 v% mixtures of tris with (A) DMSO, (B) ethanol, and (C) HFIP with and without NaOH titration. Insets are zoomed in plots of the first 200 seconds of the reaction. (D) Calculated reaction rate of pNA hydrolysis in each given condition, with background rates subtracted. (E) Direct comparison of the kinetic activity curves for the most comparable conditions in each solvent system, identified by a * in panel D. Peptide concentration was 20 μM and substrate concentration was 200 μM in all conditions.

ASSOCIATED CONTENT

Supporting Information

Kinetic curves of p-NA background hydrolysis in different temperatures and solvents, DSC calibration using lysozyme, integration intensities from 2D IR experiments, molecular dynamic simulations to derive hydrogen bond lifetimes, and calculated extinction coefficients in varying solvent conditions can be found in the supporting information. This material is available free of charge *via* the Internet at http://pubs.acs.org.

AUTHOR INFORMATION

Corresponding Author

*E-mail: christopher.so@nrl.navy.mil

Present Addresses

† Formerly at NRL

Author Contributions

A.B.G., A.D.D. and J.C.O. developed and calibrated 2DIR instrumentation. M.A.B. and C.R.S. performed enzyme assays, M.A.B. developed thermodynamic modeling. M.A.B and C.R.S. collected AFM images of fibrils. M.A.B. performed FTIR experiments across temperatures. A.D.D., E.S.R., and J.C.O. performed 2DIR measurements in solvents and across temperatures. E.S.R. developed 2DIR quantitation tools. M.D.T. and J.G.L. developed DSC methods for proteins. K.P.F. performed molecular dynamics simulations. C.R.S., M.A.B and A.D.D. wrote the manuscript; E.S.R., K.P.F., and M.D.T. participated in manuscript preparation. C.R.S. conceived and directed the overall project.

ACKNOWLEDGMENT

This work was funded by the Office of Naval Research through the Naval Research Laboratory Base Program. The authors would like to thank Michael C. Wilson for discussions on temperature dependent activity.

ABBREVIATIONS

Additional Information

The author(s) declare no competing financial interests.

REFERENCES

1. van den Burg, B., Extremophiles as a source for novel enzymes. *Curr Opin Microbiol* **2003,** *6* (3), 213-218.
2. Demirjian, D. C.; Moris-Varas, F.; Cassidy, C. S., Enzymes from extremophiles. *Curr Opin Chem Biol* **2001,** *5* (2), 144-151.
3. Chapman, M. R.; Robinson, L. S.; Pinkner, J. S.; Roth, R.; Heuser, J.; Hammar, M.; Normark, S.; Hultgren, S. J., Role of Escherichia coli curli operons in directing amyloid fiber formation. *Science* **2002,** *295* (5556), 851-855.
4. Mackay, J. P.; Matthews, J. M.; Winefield, R. D.; Mackay, L. G.; Haverkamp, R. G.; Templeton, M. D., The hydrophobin EAS is largely unstructured in solution and functions by forming amyloid-like structures. *Structure* **2001,** *9* (2), 83-91.
5. Barlow, D. E.; Dickinson, G. H.; Orihuela, B.; Kulp, J. L.; Rittschof, D.; Wahl, K. J., Characterization of the Adhesive Plaque of the Barnacle Balanus amphitrite: Amyloid-Like Nanofibrils Are a Major Component. *Langmuir* **2010,** *26* (9), 6549-6556.
6. Kayser, J. J.; Arnold, P.; Steffen-Heins, A.; Schwarz, K.; Keppler, J. K., Functional ethanol-induced fibrils: Influence of solvents and temperature on amyloid-like aggregation of beta-lactoglobulin. *J Food Eng* **2020,** *270*.
7. Loveday, S. M.; Wang, X. L.; Rao, M. A.; Anema, S. G.; Singh, H., beta-Lactoglobulin nanofibrils: Effect of temperature on fibril formation kinetics, fibril morphology and the rheological properties of fibril dispersions. *Food Hydrocolloids* **2012,** *27* (1), 242-249.
8. Maury, C. P. J., Amyloid and the origin of life: self-replicating catalytic amyloids as prebiotic informational and protometabolic entities. *Cell Mol Life Sci* **2018,** *75* (9), 1499-1507.
9. Pelin, J. N. B. D.; Gerbelli, B. B.; Soares, B. M.; Aguilar, A. M.; Alves, W. A., Amyloidogenic model peptides as catalysts for stereoselective aldol reactions. *Catal Sci Technol* **2019,** *9* (16), 4304-4313.
10. Chatterjee, A.; Mahato, C.; Das, D., Complex Cascade Reaction Networks via Cross beta Amyloid Nanotubes. *Angew Chem Int Edit* **2021,** *60* (1), 202-207.
11. Makhlynets, O. V.; Gosavi, P. M.; Korendovych, I. V., Short Self-Assembling Peptides Are Able to Bind to Copper and Activate Oxygen. *Angew Chem Int Edit* **2016,** *55* (31), 9017-9020.
12. Rufo, C. M.; Moroz, Y. S.; Moroz, O. V.; Stohr, J.; Smith, T. A.; Hu, X. Z.; DeGrado, W. F.; Korendovych, I. V., Short peptides self-assemble to produce catalytic amyloids. *Nat Chem* **2014,** *6* (4), 303-309.
13. Zozulia, O.; Dolan, M. A.; Korendovych, I. V., Catalytic peptide assemblies. *Chem Soc Rev* **2018,** *47* (10), 3621-3639.
14. Lengyel, Z.; Rufo, C. M.; Moroz, Y. S.; Makhlynets, O. V.; Korendovych, I. V., Copper-Containing Catalytic Amyloids Promote Phosphoester Hydrolysis and Tandem Reactions. *Acs Catal* **2018,** *8* (1), 59-62.
15. Rout, S. K.; Friedmann, M. P.; Riek, R.; Greenwald, J., A prebiotic template-directed peptide synthesis based on amyloids. *Nature communications* **2018,** *9* (1), 1-8.
16. Jaworek, M. W.; Schuabb, V.; Winter, R., Pressure and cosolvent modulation of the catalytic activity of amyloid fibrils. *Chem Commun* **2018,** *54* (45), 5696-5699.
17. Knierbein, M.; Wangler, A.; Luong, T. Q.; Winter, R.; Held, C.; Sadowski, G., Combined co-solvent and pressure effect on kinetics of a peptide hydrolysis: an activity-based approach. *Physical Chemistry Chemical Physics* **2019,** *21* (40), 22224-22229.

18. Ostermeier, L.; de Oliveira, G. A. P.; Dzwolak, W.; Silva, J. L.; Winter, R., Exploring the polymorphism, conformational dynamics and function of amyloidogenic peptides and proteins by temperature and pressure modulation. *Biophysical Chemistry* **2021,** *268*.
19. Luong, T. Q.; Erwin, N.; Neumann, M.; Schmidt, A.; Loos, C.; Schmidt, V.; Fandrich, M.; Winter, R., Hydrostatic Pressure Increases the Catalytic Activity of Amyloid Fibril Enzymes. *Angew Chem Int Edit* **2016,** *55* (40), 12412-12416.
20. Barth, A.; Zscherp, C., What vibrations tell us about proteins. *Q Rev Biophys* **2002,** *35* (4), 369-430.
21. Zandomeneghi, G.; Krebs, M. R. H.; Mccammon, M. G.; Fandrich, M., FTIR reveals structural differences between native beta-sheet proteins and amyloid fibrils. *Protein Sci* **2004,** *13* (12), 3314-3321.
22. Sarroukh, R.; Goormaghtigh, E.; Ruysschaert, J. M.; Raussens, V., ATR-FTIR: A "rejuvenated" tool to investigate amyloid proteins. *Bba-Biomembranes* **2013,** *1828* (10), 2328-2338.
23. Moran, S. D.; Zanni, M. T., How to Get Insight into Amyloid Structure and Formation from Infrared Spectroscopy. *J Phys Chem Lett* **2014,** *5* (11), 1984-1993.
24. Lomont, J. P.; Ostrander, J. S.; Ho, J. J.; Petti, M. K.; Zanni, M. T., Not All beta-Sheets Are the Same: Amyloid Infrared Spectra, Transition Dipole Strengths, and Couplings Investigated by 2D IR Spectroscopy. *J Phys Chem B* **2017,** *121* (38), 8935-8945.
25. Lomont, J. P.; Rich, K. L.; Maj, M.; Ho, J. J.; Ostrander, J. S.; Zanni, M. T., Spectroscopic Signature for Stable beta-Amyloid Fibrils versus beta-Sheet-Rich Oligomers. *J Phys Chem B* **2018,** *122* (1), 144-153.
26. Yates, E. A.; Legleiter, J., Preparation Protocols of A beta(1-40) Promote the Formation of Polymorphic Aggregates and Altered Interactions with Lipid Bilayers. *Biochemistry-Us* **2014,** *53* (45), 7038-7050.
27. Stine, W. B.; Dahlgren, K. N.; Krafft, G. A.; LaDu, M. J., In vitro characterization of conditions for amyloid-beta peptide oligomerization and fibrillogenesis. *Journal of Biological Chemistry* **2003,** *278* (13), 11612-11622.
28. Heier, J. L.; Mikolajczak, D. J.; Bottcher, C.; Koksch, B., Substrate specificity of an actively assembling amyloid catalyst. *Biopolymers* **2017,** *108* (1).
29. Grafton, A. B.; Dunkelberger, A. D.; Simpkins, B. S.; Triana, J. F.; Hernandez, F. J.; Herrera, F.; Owrutsky, J. C., Excited-state vibration-polariton transitions and dynamics in nitroprusside. *Nature Communications* **2021,** *12* (1).
30. Best, R. B.; Zhu, X.; Shim, J.; Lopes, P. E. M.; Mittal, J.; Feig, M.; MacKerell, A. D., Optimization of the Additive CHARMM All-Atom Protein Force Field Targeting Improved Sampling of the Backbone phi, psi and Side-Chain chi(1) and chi(2) Dihedral Angles. *J Chem Theory Comput* **2012,** *8* (9), 3257-3273.
31. Becke, A. D., Density-Functional Thermochemistry .3. The Role of Exact Exchange. *J Chem Phys* **1993,** *98* (7), 5648-5652.
32. Hess, B.; Bekker, H.; Berendsen, H. J. C.; Fraaije, J. G. E. M., LINCS: A linear constraint solver for molecular simulations. *J Comput Chem* **1997,** *18* (12), 1463-1472.
33. Luzar, A.; Chandler, D., Hydrogen-bond kinetics in liquid water. *Nature* **1996,** *379* (6560), 55-57.
34. Feller, G.; Gerday, C., Psychrophilic enzymes: Hot topics in cold adaptation. *Nat Rev Microbiol* **2003,** *1* (3), 200-208.

35. Siddiqui, K. S., Some like it hot, some like it cold: Temperature dependent biotechnological applications and improvements in extremophilic enzymes. *Biotechnol Adv* **2015,** *33* (8), 1912-1922.
36. Arcus, V. L.; Prentice, E. J.; Hobbs, J. K.; Mulholland, A. J.; Van der Kamp, M. W.; Pudney, C. R.; Parker, E. J.; Schipper, L. A., On the Temperature Dependence of Enzyme-Catalyzed Rates. *Biochemistry-Us* **2016,** *55* (12), 1681-1688.
37. Hobbs, J. K.; Jiao, W. T.; Easter, A. D.; Parker, E. J.; Schipper, L. A.; Arcus, V. L., Change in Heat Capacity for Enzyme Catalysis Determines Temperature Dependence of Enzyme Catalyzed Rates. *Acs Chem Biol* **2013,** *8* (11), 2388-2393.
38. Cho, M., Vibrational solvatochromism and electrochromism: Coarse-grained models and their relationships. *J Chem Phys* **2009,** *130* (9).
39. Blasiak, B.; Lee, H.; Cho, M., Vibrational solvatochromism: Towards systematic approach to modeling solvation phenomena. *J Chem Phys* **2013,** *139* (4).
40. Capasso, C.; De Luca, V.; Carginale, V.; Cannio, R.; Rossi, M., Biochemical properties of a novel and highly thermostable bacterial alpha-carbonic anhydrase from Sulfurihydrogenibium yellowstonense YO3AOP1. *J Enzym Inhib Med Ch* **2012,** *27* (6), 892-897.
41. Alaei, L.; Moosavi-Movahedi, A. A.; Hadi, H.; Saboury, A. A.; Ahmad, F.; Amani, M., Thermal Inactivation and Conformational Lock of Bovine Carbonic Anhydrase. *Protein Peptide Lett* **2012,** *19* (8), 852-858.
42. Romans, A. Y.; Graichen, M. E.; Lochmuller, C. H.; Henkens, R. W., Kinetics and Mechanism of Dissociation of Zinc Ion from Carbonic-Anhydrase. *Bioinorg Chem* **1978,** *9* (3), 217-229.
43. Buck, M., Trifluoroethanol and colleagues: cosolvents come of age. Recent studies with peptides and proteins. *Q Rev Biophys* **1998,** *31* (3), 297-355.
44. Jasanoff, A.; Fersht, A. R., Quantitative-Determination of Helical Propensities from Trifluoroethanol Titration Curves. *Biochemistry-Us* **1994,** *33* (8), 2129-2135.
45. Sonnichsen, F. D.; Vaneyk, J. E.; Hodges, R. S.; Sykes, B. D., Effect of Trifluoroethanol on Protein Secondary Structure - an Nmr and Cd Study Using a Synthetic Actin Peptide. *Biochemistry-Us* **1992,** *31* (37), 8790-8798.

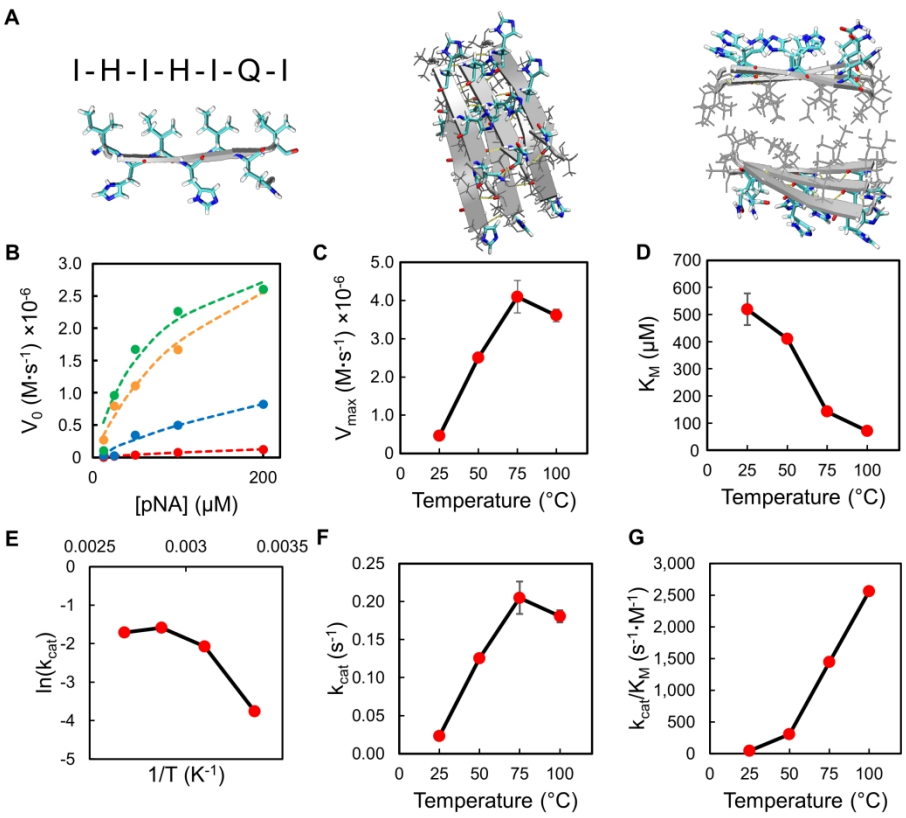

Figure 1. Molecular structure and temperature dependent activity of catalytic amyloids formed from IHIHIQI. (A) Structure of the IHIHIQI peptide (left), along with structures of the assembled catalytic amyloids (center, right). (A) Initial velocity v0 as a function of p-nitrophenyl acetate concentration across temperatures (red, 25 °C, blue, 50 °C, orange, 75 °C, green 100 °C), (B) Vmax calculated as a function of temperature, (C) Michaelis constant (KM) as a function of temperature, (D) Arrhenius relation plotted as 1/T versus ln(kcat), (E) Catalytic turnover (kcat) calculated as Vmax/[IHIHIQI] plotted across temperature, and (F) catalytic efficiency of catalytic amyloids showing optimum at 75 °C. Peptide concentration is 20 μM in all cases, and substrate concentrations include 12.5, 25, 50, 100, and 200 μM. All experiments performed in triplicate.

230x190mm (300 x 300 DPI)

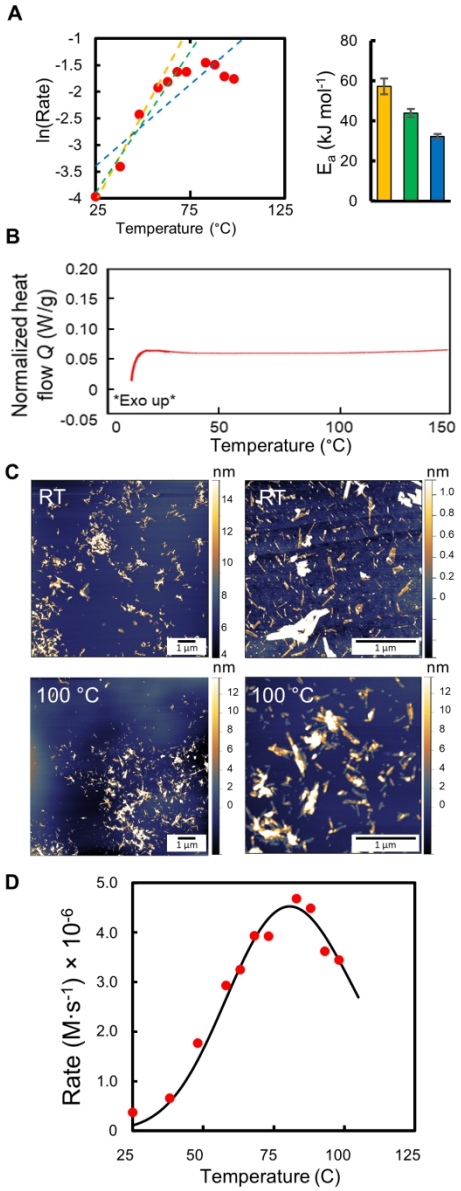

Figure 2. Catalytic amyloids maintain structure and function at high temperatures. (A) Temperature-dependent activity curves fit to the Arrhenius equation to derive the activation energy. Dashed lines represent linear fits for the activity curve in the temperature range 25-50°C (yellow), 25-80 °C (green), and 25-100 °C (blue). (B) DSC curve of IHIHIQI fibril solution. (C) Representative AFM images of fibrils at room temperature (top) and 100 °C (bottom), with zoomed images presented on the right. (D) Same activity data as (A) fit to the MMRT equation. Experiments were performed in triplicate and error bars for the activation energy represent the standard deviation.

102x243mm (300 x 300 DPI)

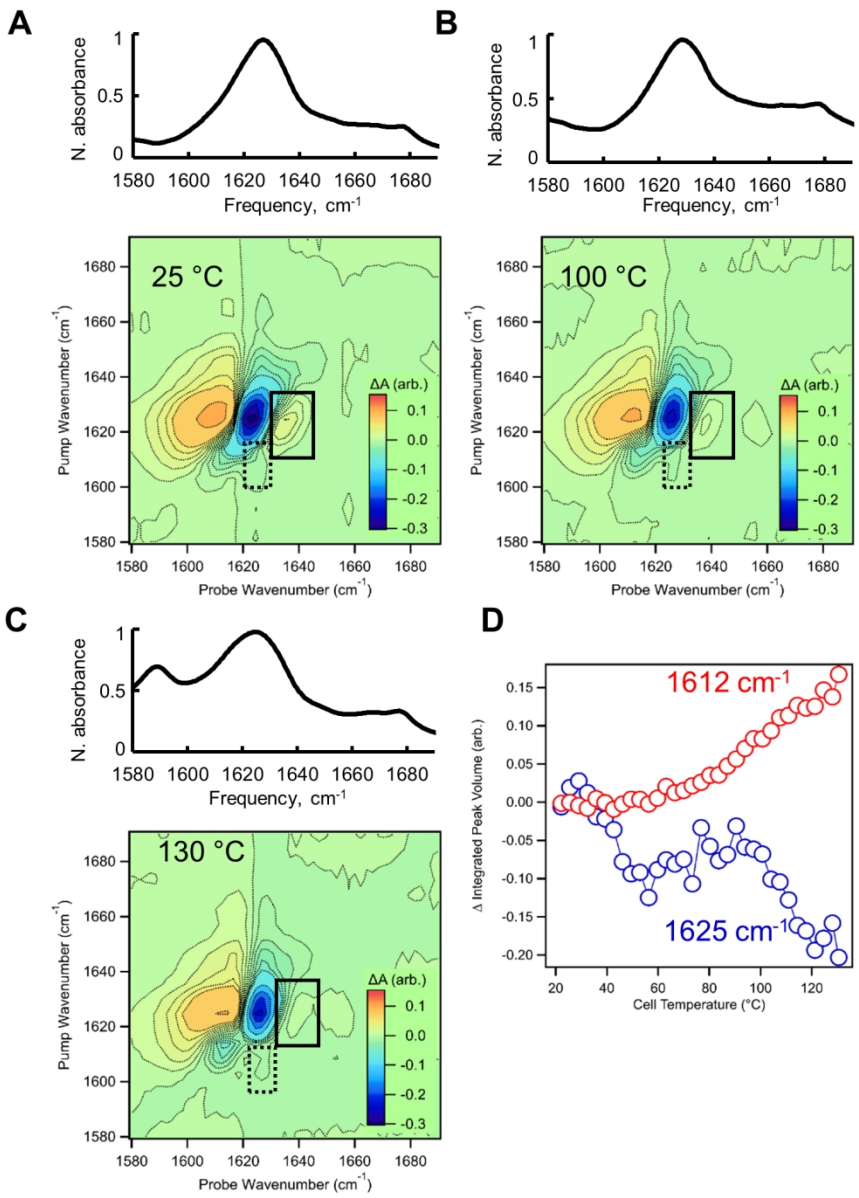

Figure 3 Linear IR (top) and 2DIR (bottom) spectra of IHIHIQI in D2O recorded at cell temperatures (A) 25 °C, (B) 100 °C and (C) 130 °C. The contour line spacing is unequal with more contours between values of -0.1 and 0.1 to accentuate small features in the spectra. The solid black boxes highlight the cross peak denoted 1625/1635 in the text and the dashed black boxes highlight the cross peak denoted 1612/1625. (D) Differential peak volume computed as described in the main text of the two main features at 1625 cm-1 (blue) and 1612 cm-1 (red) as a function of the temperature of the cell.

133x175mm (300 x 300 DPI)

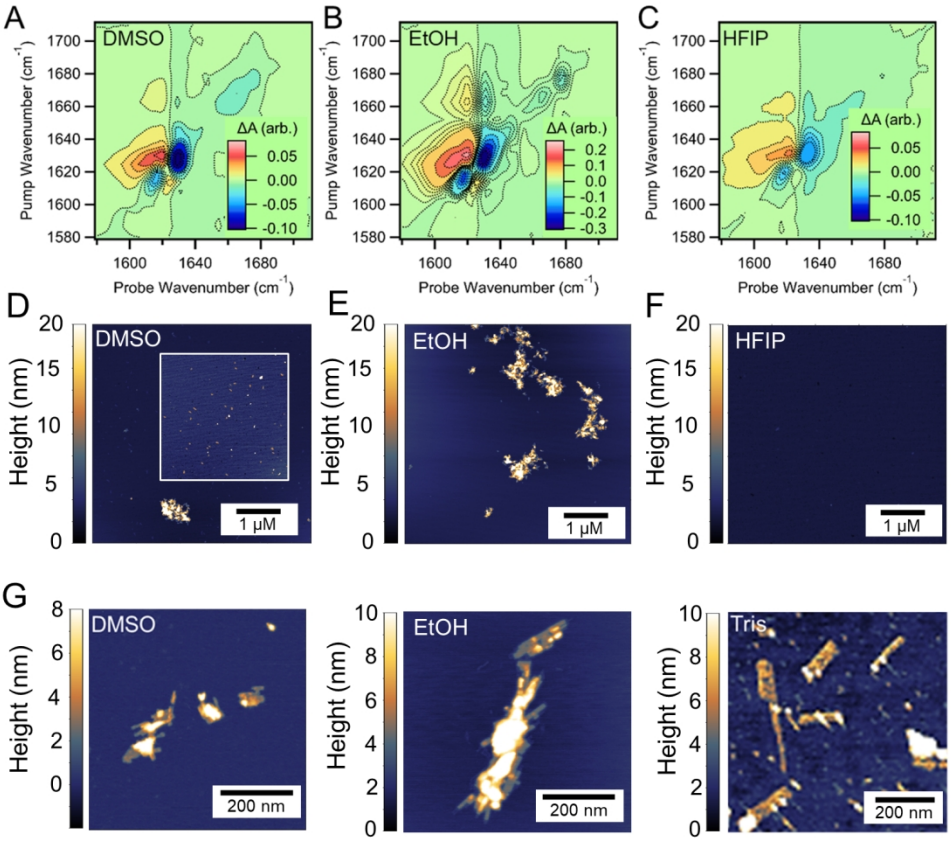

Figure 4. Structure of catalytic amyloids in non-aqueous co-solvents. 2DIR spectra of IHIHIQI in (A) DMSO, (B) ethanol, and (C) HFIP. The contour line spacing is unequal with more contours between values of -0.1 and 0.1 to accentuate small features in the spectra. Representative AFM images of IHIHIQI in (D) DMSO, (E) ethanol, and (F) HFIP. The box-in portion in panel (D) has a smaller height scale in order to see the shorter aggregates more clearly. (G) Belt-like amyloid fibrils of IHIHIQI present in 50/50 vol% tris/DMSO, tris/EtOH, and 100% tris buffer.

143x124mm (300 x 300 DPI)

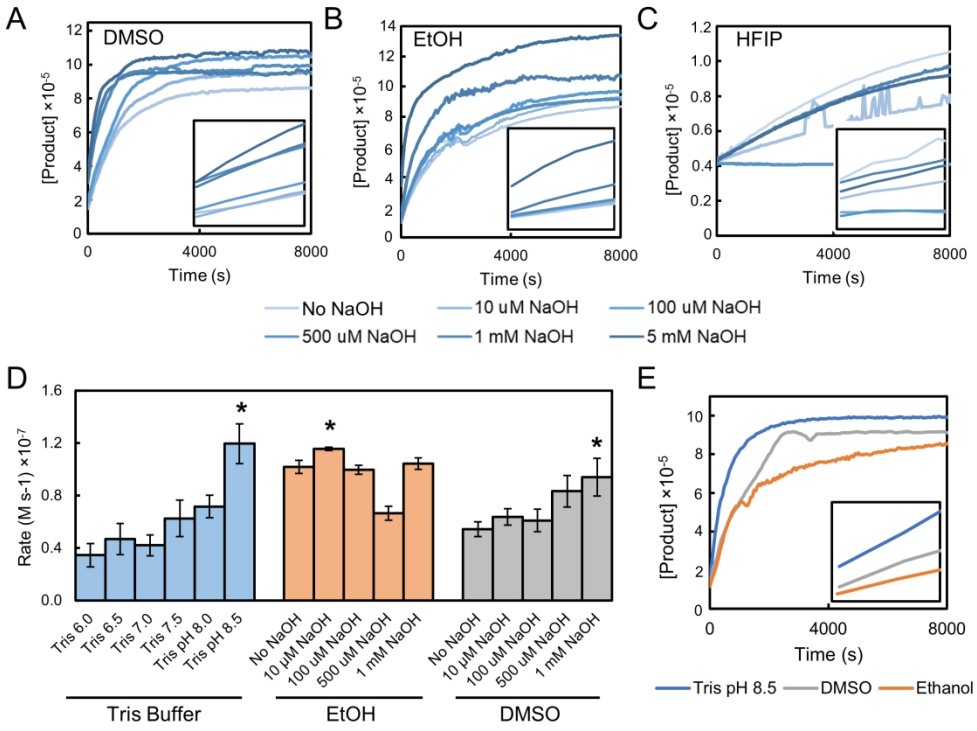

Figure 5. Activity of catalytic amyloids in non-aqueous co-solvents. Activity of IHIHIQI fibrils toward pNA in 50/50 v% mixtures of tris with (A) DMSO, (B) ethanol, and (C) HFIP with and without NaOH titration. Insets are zoomed in plots of the first 200 seconds of the reaction. (D) Calculated reaction rate of pNA hydrolysis in each given condition, with background rates subtracted. (E) Direct comparison of the kinetic activity curves for the most comparable conditions in each solvent system, identified by a * in panel D. Peptide concentration was 20 μM and substrate concentration was 200 μM in all conditions.

206x152mm (300 x 300 DPI)